PCCP

RSC Publishing

PAPER

View Article Online
View Journal

Cite this: DOI: 10.1039/c3cp50644d

Systematic evaluation of fluorescence correlation spectroscopy data analysis on the nanosecond time scale†

Katrin Steger,[a] Stefan Bollmann,[a] Frank Noé[b] and Sören Doose*[a]

Received 12th February 2013,
Accepted 26th April 2013

DOI: 10.1039/c3cp50644d

www.rsc.org/pccp

Signal fluctuations in a fluorescence time trace on nanosecond time scales can be induced by specific quenching interactions that report on the dynamics of biomolecules. Fluorescence correlation spectroscopy is an analysis tool to investigate dynamic processes on time scales from pico- to milliseconds or longer. Under certain conditions, *e.g.* in a solvent of high viscosity, a fluorescence labeled dynamic biomolecule yields multiple independent correlation decays due to rotational and translational diffusion, fluorescence quenching interactions, and fluorophore photophysics. We compared parameter estimation for FCS data with multiple correlation decays by dynamical fingerprint analysis and by the non-linear Levenberg–Marquardt fitting procedure and identified conditions for which dynamical fingerprint analysis can be of advantage. In this context we identified a previously unrecognized photophysical process in ATTO655 that introduces fluorescence intermittency on nanosecond time scales that is absent in MR121. The optimized fitting procedure is used to resolve the viscosity dependence of fluorescence quenching for photoinduced electron transfer probes.

Introduction

Fluorescence correlation spectroscopy (FCS) has become an important data analysis method for the investigation of molecular properties ranging from hydrodynamic radii to conformational dynamics.[1–9] By probing stochastic signal fluctuations of a low concentrated sample in thermodynamic equilibrium, *e.g.* due to fluorescence quenching interactions of well-designed and site-specifically incorporated reporter molecules, FCS has been advantageously used to monitor conformational dynamics of biomolecules and characterize protein dynamics. Fluorescence fluctuations nowadays can be observed with exquisite sensitivity and analyzed simultaneously over orders of magnitude in time ranging from picoseconds to minutes. Progress is due to technical advances including the use of confocal microscopy for efficient fluorescence detection, precisely timed single-photon recording, and efficient correlation algorithms or hardware devices for multiple-tau correlation analysis, among others.[10–13] Cross-correlation of two single-photon avalanche photodiode detectors combined with the use of appropriate spectral filters ensures an optimized signal-to-noise ratio and eliminates contributions from detector dead-times and afterpulsing on correlations at nanosecond lag times (τ_{lag}). Hardware correlation electronics and software correlation algorithms based on multiple-tau correlation analysis are commercially available, in which the temporal resolution of the correlation curve ($\Delta\tau_{lag}$) is iteratively adjusted to the absolute lag time. That way the total number of computations needed for generating a correlation curve over many orders of magnitude in time is reduced and the acquisition of FCS data in real time is possible.

At small lag times FCS is limited by the antibunching signature that results from the finite fluorescence radiation rate of the fluorescing molecules.[14,15] Due to the quantum mechanical properties of a two state system, a single emitter cannot emit multiple photons simultaneously; a fact that results in an anticorrelation with a rise time on the order of the fluorescence lifetime (typically few nanoseconds). At large lag times most FCS experiments are limited by the fact that the instrumental stability is compromised by temperature variations and slow changes in the observation volume, for example due to shifts in the focal plane alignment. Apart from these limitations, fluorescence fluctuations are indicative of various interesting molecular processes, such as reorientation due to

[a] Department of Biotechnology and Biophysics, Biocenter, Am Hubland, Julius-Maximilians University, 97074 Würzburg, Germany. E-mail: soeren.doose@uni-wuerzburg.de; Fax: +49 931 3184509
[b] Research Center Matheon, FU Berlin, Arnimallee 6, 14159 Berlin, Germany

† Electronic supplementary information (ESI) available: Fig. S1–S6. See DOI: 10.1039/c3cp50644d

translational and rotational diffusion or from conformational dynamics that change the local environment of a fluorophore and the related fluorescence quantum yield. Often there is particular interest for fluctuations on the nano- and microsecond time scale. When monitoring fluorescent organic dyes diffusing in aqueous solution, nanosecond signal fluctuations are typically introduced by antibunching in the single fluorophore emission, rotational diffusion of the fluorophore in the polarized field of the excitation laser, photophysical processes such as the population of long-lived triplet states by intersystem crossing, or fluorescence quenching upon interaction between the fluorophore and nearby quenching moieties. In many experiments a fluorescent moiety is in close proximity to a fluorescence quenching moiety and changes in their relative distance or orientation influence the intensity of emitted fluorescence. van der Waals contact of an organic fluorophore and its quencher can be probed *e.g.* by photoinduced electron transfer (PET), dimerization, or other interactions that change the excited state probability distribution for radiative or non-radiative transitions to the ground state.[16–24] Distance changes between solvent-separated probes around a few nanometers can be monitored by Förster resonance energy transfer.[25–31]

The difficulty in analyzing the FCS data lies in identifying an appropriate theoretical model describing the molecular processes that have generated the fluorescence fluctuations, fitting it to the data, and obtaining relevant information from the model parameters. The most common approach to analyze correlation data is to employ χ-square minimizing non-linear fitting routines such as the Levenberg–Marquardt (LM) algorithm in order to optimize the parameters of a user-defined analytical expression for the correlation function. The expression for the correlation function usually results from a physical model containing the molecular and photophysical processes influencing the experimental correlation data. Typically, such a model contains a fixed number of prescribed exponential decay processes, either due to photophysical or molecular state transitions that cause a decorrelation of the fluorescence at different timescales. The reliability of the fitting routine may be increased by constraining fit parameters to reasonable intervals or by fixing them to constant values that are determined in independent experiments. Simultaneous fitting of multiple correlation curves with the same parameters is another approach to reduce the statistical uncertainty of the fitting results. Stochastic approaches were developed to enable high-throughput fitting procedures independent of manually chosen starting values.[32] Model functions are also optimized in a more general way by using maximum likelihood estimation or maximum entropy methods. For rating a finite number of competing model functions Bayesian inference testing was employed.[33,34]

An alternative to fitting prescribed model functions with a fixed number of exponentials is to use methods that estimate the amplitude density of the rate or timescale spectrum.[35–38] It can be shown that in the absence of statistical noise, the amplitude density of the rate spectrum, also known as the power spectrum, is the forward Laplace transform of the correlation function, while the amplitude density of the timescale spectrum, also called ''dynamical fingerprint'', is the inverse Laplace transform of the correlation function.[35] The rationale for estimating the density of timescales rather than prescribing a fixed number of exponential relaxations is that the correlation function resulting from fluorescence changes due to conformational dynamics can be shown to be a sum of exponential decays, each with a timescale of an equilibrium conformational transition.[35,39] Photophysical state transitions add more exponential decays. For each molecule, there are infinitely many such processes. Only if the slow processes are separated in time from the fast processes, such as in a system with so-called two- or three-state kinetics, the spectrum has clearly separated peaks with distinct features. Estimating the dynamical fingerprint from the data, rather than enforcing a model with a certain number of states, avoids enforcing the number of conformational states in advance, and offers the chance of finding unexpected processes. However, the ability to resolve subtle features – such as peaks with small amplitudes, or separation of nearby peaks – is still limited by noise and the fundamental problem that calculating the spectrum from a correlation function is mathematically poorly conditioned. Additionally, noise may produce spurious peaks in the estimated spectrum, and it is hence very important to ensure a good signal-to-noise ratio by calculating the FCS function from a large dataset. The estimation of the rate spectrum or dynamical fingerprint is usually done using error-minimization or likelihood-maximization approaches, often using regularizations such as maximum entropy[36] or prior probabilities[37] to avoid overfitting the data.

In this work we analyzed FCS data that report on bimolecular PET-based quenching interactions of freely diffusing oxazine fluorophores (MR121 or ATTO655) and quencher molecules (tryptophan, Trp) with characteristic time constants of tens to hundreds of nanoseconds.[24,40,41] When monitoring these processes at increased viscosity, as is of interest for instance when using PET probes to understand the relationship between polymer dynamics and solvent conditions,[42] rotational diffusion of the fluorophore electronic transition dipoles adds an additional correlation decay. We found that standard fitting procedures are not reliable for extracting all parameters from such complex experimental FCS correlation curves. We therefore tested for systematic deviations that arise when analyzing FCS data for model systems with multiple decays on time scales close to the antibunching signature. We analyzed either experimental FCS data for bimolecular interactions between fluorophore and Trp freely diffusing in aqueous sugar solutions or simulated correlation data. We determined conditions under which LM fitting and dynamic fingerprint analysis yield reliable parameter estimates. We further demonstrate that the dynamical fingerprint analysis can be advantageous under the given conditions for analyzing FCS data with multiple decay components. Our results have implications for FCS analysis of dynamic processes on nano- to millisecond time scales such as that applied in many single-molecule fluorescence studies of dynamic biomolecules.

Materials and methods

Experimental FCS

FCS measurements were performed on an inverted microscope (IX71, Olympus Deutschland GmbH, Hamburg, Germany) with custom-made modifications. Fluorophores were excited in the visible red light spectrum at 640 nm using a diode laser (OBIS640, Coherent Europe B.V., Utrecht, Netherlands; in combination with a clean-up filter) that was coupled to an oil-immersion objective (U Plan S Apo 60×, 1.35 NA; Olympus) using a dichroic beam splitter (645DLRP; Omega Optics; Brattleboro, VT, USA). The laser power was adjusted to around 800 μW as measured at the back aperture of the objective. The fluorescence signal was collected using the same objective, filtered using a band-pass filter (700DF75, Chroma Technology Corporation, Bellows Falls, VT, USA), split into two detection channels using a 50 : 50 non-polarizing beam splitter cube (Thorlabs GmbH, Munich, Germany), and imaged on two multi-mode optical fibers with an entrance diameter of 100 μm that served as a confocal pinhole. Fibers were coupled to the active areas of two avalanche photodiodes (APD, SPCM-AQR-14-FC; PerkinElmer, USA) and signals were recorded as single-photon time traces (typically 15 min) in TTTR mode using data acquisition electronics (PicoHarp 300, PicoQuant GmbH, Berlin, Germany) and software (SymPhoTime Version 5.3.2, PicoQuant). Fluorescence photons were shared by two APDs and analyzed in cross-correlation mode in order to eliminate effects from detector dead-times and afterpulsing. Cross-correlation functions of the two recorded time traces were calculated using SymPhoTime (PicoQuant). Multiple-tau correlation functions were generated from a minimal lag time of τ_{min} = 18 ps to a maximum lag time of τ_{max} = 0.9 s with the number of lag times with equal lag time steps $\Delta\tau$ being N = 8. The temperature was controlled to (20 ± 1) °C by heating/cooling the objective using a custom-made Peltier element. All premixed samples were transferred onto microscope slides with a small depression and covered by a cover slip.

As a model system we present data for the bimolecular quenching interaction between the organic fluorophore MR121 (provided by Prof. K.-H. Drexhage, Siegen University) or ATTO655 (AttoTec GmbH, Siegen, Germany) and the amino acid tryptophan (Trp; Sigma-Aldrich Chemie GmbH, Munich, Germany). Static quenching occurs upon formation of bimolecular complexes through a photoinduced electron transfer process.[24,40,43] FCS data were recorded for samples with a dye concentration close to 1 nM and Trp concentrations of 10 mM. The buffer was a mixture of phosphate buffered saline (PBS, pH 7.3) with various amounts of sucrose and 0.5% detergent (Tween20, Sigma) to reduce adhesion on the glass surface. Sucrose concentrations were checked by measurements of the refractive index (DR201-95, A. Krüss Optronik, Hamburg, Germany) and the corresponding viscosity was determined from tabulated literature values.[44]

Data simulation

All data generation and analysis were carried out using the computer software package Mathematica (Version 8.0.1., Wolfram Research Inc., Champaign, IL, USA). Two sets of data simulations were carried out; either FCS data were directly modeled or were calculated from a discrete-time Markov chain. In the first approach FCS data curves were generated starting with a model function of the form

$$G(\tau) = 1 + \sum_{i=1}^{n} G_i(\tau) = 1 + \sum_{i=1}^{n} a_i e^{-k_i \tau} \quad (1)$$

including n (here two or more) exponential decay components with amplitudes a_i and characteristic rate constants k_i (inverse characteristic time constants τ_i) for each decay component.

In order to simulate the typical multiple-tau experimental setup, the model function was evaluated at a non-uniform series of τ-values (lag time). We generated a quasi-logarithmic discrete lag time scale by doubling the lag time increments $\Delta\tau$ every L channels. Starting with a minimum lag time τ_{min} = 100 ps, the first doubling was performed after L = 16 channels and followed by subsequent doubling every L = 8 channels until a series with 200 elements was calculated. The maximum lag time is about one millisecond (τ_{max} = 0.94 ms). This lag time series generated with L = (16, 8, 8,. . ., 8) is typical for many FCS hardware and software correlators since it was shown to minimize triangular averaging distortions and thus to be optimal with respect to resolution and signal-to-noise aspects.[13,45]

Noise was generated using a random number generator (Mathematica 8.0.1) for normally distributed numbers that were added to the model function. The normally distributed noise was adjusted for each lag time to follow the typical scaling behavior given a certain noise amplitude c:

$$\mathrm{stddev(noise)} = c\frac{1}{\sqrt{\tau}}, \quad \mathrm{mean(noise)} = 0. \quad (2)$$

It was shown previously that this relation is due to shot noise, influences from background, and detector noise[45,46] and holds for our experimental FCS data up to a lag time of ~10 μs.[35] The adjustable parameter for the noise amplitude c was estimated from experimental data and accordingly varied in simulations between 10^{-6} and 10^{-4} $s^{1/2}$.

Since the latter approach neglects the fact that in real multiple-tau FCS data noise at different lag times is correlated, we also performed simulations of Markov-chains according to a photophysical model with transitions between a ground (state 1), excited (state 2), and dark state (state 3). We used rate constants according to the three-dimensional transition matrix M = ((0, 0.3, 0), (0.3, 0, 0.1), (0.1, 0, 0)). Single-photon time series were generated by assuming that only transitions from the excited to the ground state result in photon detection. Poisson-distributed background photons were added to this photon time series and correlation functions were calculated using a multiple-tau correlation algorithm as described.[45,47] In none of the data simulations a correlation decay due to translational diffusion was included.

Data analysis

Simulated and experimental data were fitted using a least-squares non-linear Levenberg–Marquardt (LM) fitting routine

as implemented in Mathematica (Version 8.0.1.) or as implemented in Origin (Version 8.5, OriginLab Corporation, Northampton, MA, USA). The following fit model was used:

$$G(\tau) = G_D(\tau)(1 - Ae^{-k_{ab}\tau} + Re^{-k_{rot}\tau} + Ke^{-k_{rel}\tau} + Te^{-k_{trip}\tau}) \quad (3)$$

with $G_D(\tau) = 1$ when fitting simulated data or with

$$G_D(\tau) = N^{-1}\left(1 - \frac{\tau}{\tau_D}\right)^{-1} \quad (4)$$

when fitting experimental data at full length of the correlation curve. Here N is the average number of molecules in the observation volume and $\tau_D = \omega_{xy}^2/4D$ is the average diffusion time for molecules to pass through the observation volume (with lateral dimension ω_{xy}) by translational diffusion according to the diffusion constant D.[3,48] All other parameters in eqn (3) and throughout the manuscript are as follows: A, $k_{ab} = \tau_{ab}^{-1}$ are amplitude and rate/time constant for the antibunching process; R, $k_{rot} = \tau_{rot}^{-1}$ for rotational diffusion; K, $k_{rel} = \tau_{rel}^{-1}$ for contact-induced quenching; T, $k_{isc} = \tau_{isc}^{-1}$ for intersystem crossing from the excited singlet to long-lived triplet states.

Dynamical fingerprints were determined as described previously[35] using the algorithm implemented in JAVA and included in the scimex package (version of Feb 2011, https://simtk.org/home/scimex). In this version, the diffusion part $G_D(\tau)$ of the correlation function is included in the fingerprint determination as an independent and analytical expression. Here, fingerprints were determined using an updated version of the computer code that included a similar treatment of the antibunching signature using an analytical expression:

$$G(\tau) = G_D(\tau)\left(1 - Ae^{-k_{ab}\tau} + \int_{t=0}^{\infty} \gamma(t)e^{-\tau/t}\right). \quad (5)$$

where A and k_{ab} are the parameters of the antibunching term and $\gamma(t)$ is the dynamical fingerprint, *i.e.* the continuous amplitude density of relaxation timescales in the data. In the dynamical fingerprint algorithm, $\gamma(t)$ is discretized in time and thus the integral in eqn (5) is approximated by a finite sum. The fingerprint fitting routine thus consisted of the following steps: (i) estimation of the diffusion component by LM fitting of $G_D(\tau)$ for $\tau > 1$ μs and effectively fixing N and τ_D accordingly during fingerprint determination; (ii) estimation of the noise amplitude c; (iii) estimation of antibunching parameters; (iv) determination of the dynamical fingerprint and fit curve by maximization of the likelihood function (for details see ref. 35).

Results

When using FCS to monitor conformational dynamics of biopolymers in aqueous solution under varying environmental conditions (temperature, viscosity, chemical additives) state of the art electronics allow the recording of a correlation function $G(\tau)$ spanning lag times from tens of picoseconds to many minutes. Under certain conditions (*e.g.* aqueous solution with 60% (w/v) sucrose at room temperature) five distinct processes can be identified when their timescales are well separated. We demonstrate this by showing $G(\tau)$ recorded for a mixture of freely diffusing Trp (10 mM) and MR121 (~1 nM), a red emitting oxazine fluorophore that is efficiently quenched by PET when forming van-der-Waals contact with Trp (Fig. 1). In the log-linear representation of $G(\tau)$ the corresponding rise or decay components include the antibunching term around a few ns, a rotational diffusion term due to rotation of the fluorophore transition dipole within the excitation laser focus around 10–20 ns, a PET-based quenching term due to contact formation of MR121 and Trp around 500 ns, a triplet term due to intersystem crossing in the fluorophore around 10–20 μs, and a translational diffusion term due to diffusional passage of the fluorophore through the laser focus around 10 ms. Estimates for the relaxation time of the exponential decay components are gained from dynamical fingerprint analysis or from fitting eqn (3) to the correlation function using a non-linear least-squares LM fitting algorithm (Fig. 1A–C) and made visible in the dynamical fingerprint shown in Fig. 1D. Very similar data are generated for short peptides or nucleotides in which one terminus is labeled with the fluorophore and the other terminus contains a quenching moiety like Trp or guanine.[49]

The dynamical processes contributing to eqn (3) are theoretically well described by physical principles. Analytical correlation functions were derived for all individual components and some combinations of them. Antibunching describes an exponential rise in the correlation time from a minimal value that depends on the number of simultaneously observed fluorescent emitters and background signal.[14,15,50–52] For a single emitter the correlation at zero lag time equals zero and the characteristic rise time is the inverse product of the excitation and the fluorescence relaxation rate constants. Rotational diffusion of individual transition dipoles for excitation and emission relates to the molecular shape of the fluorophore (and attached biomolecule) and, depending on the polarization state of the excitation light and the detectors, results in a rather complicated multi-exponential decay.[50,53–56] However, in most experimental settings, a single exponential decay is sufficient to describe the observed correlation function.[57] Under the assumption of a single excitation dipole and a negligible z-component of the excitation light field, the characteristic decay time is proportional to the rotational diffusion constant and scales with temperature and viscosity as described by the Stokes–Einstein–Debye equation $D_{rot} = k_B T/(8\pi\eta R^3)$. Fluorescence quenching due to contact-induced interactions between a fluorophore and a quenching molecule reflects the process that brings the two entities into contact. If the interaction follows a two state process with well-defined association and dissociation rate constants, a mono-exponential correlation decay emerges with a characteristic time constant that is the inverse of the sum of association and dissociation rate constants. This mono-exponential decay has indeed been observed in many PET-based quenching experiments including the bimolecular complex formation between MR121/ATTO655 and Trp (Fig. 1).[16] The population of long lived triplet states due to intersystem crossing is well understood in organic

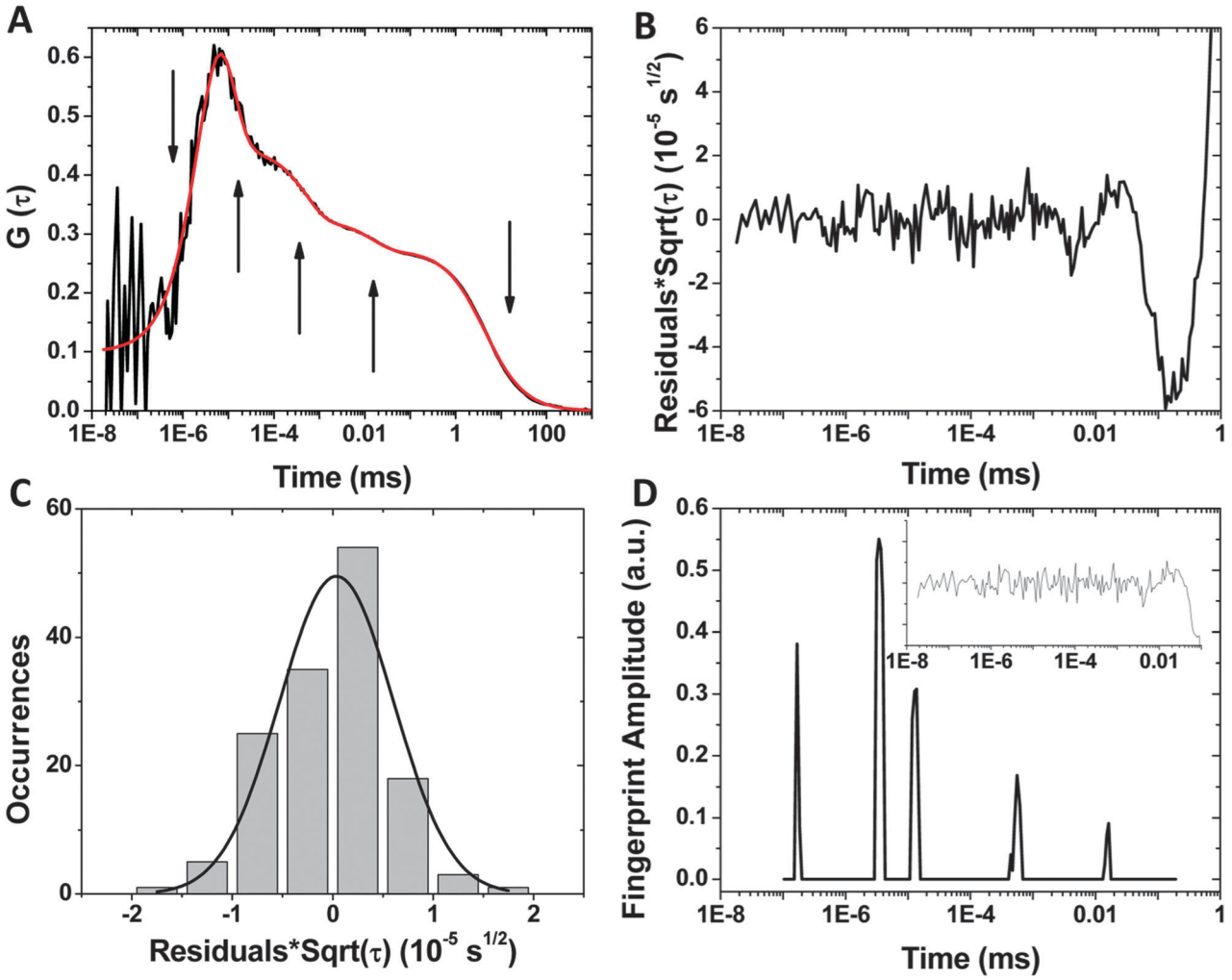

Fig. 1 FCS data representing bimolecular interactions between the freely diffusing fluorophore and the quencher. (A) FCS data generated with 1 nM MR121 and 10 mM Trp freely diffusing in a mixture of PBS buffer and 60% sucrose at 20 °C, overlaid with a fit function generated by the LM fitting routine. Arrows indicate the underlying process (from left to right): antibunching, rotational diffusion, PET-quenching, intersystem crossing, diffusion. (B) Residuals of the data fit normalized to the number of molecules N and multiplied by the square root of the lag time τ. (C) Histogram of the normalized residuals shown in (B) for the interval from 18 ps to 10 μs. The Gauss fit reveals a standard deviation with $c = 5.7 \times 10^{-6}$ $s^{1/2}$. (D) Dynamical fingerprint of data displayed in (A) with the first two peaks (from left to right) originating from the antibunching signature, third, fourth, and fifth peak originating from rotational diffusion, PET-quenching, and intersystem crossing, respectively. The inset shows residuals multiplied by $\tau^{1/2}$ for the dynamical fingerprint fit.

fluorescing molecules.[58,59] The exponential decay function that is experimentally observed can be explained by a simple approximation in which the triplet state is treated as a dark-state and the combination of ground and first electronically excited singlet states as an on-state.[60] MR121 and ATTO655 are known for small intersystem crossing rates with the result that correlation amplitudes of this process are comparably small. The correlation decay due to translational diffusion of the fluorescing entity through the excitation laser focus on millisecond time scales is well described by the classical theories on diffusional motion.[3,9,48]

With well separated time scales for all the above described processes, it is reasonable to describe the complete correlation function as a sum of exponential correlation decays combined with the standard correlation function for two-dimensional diffusion as described by eqn (3) and (4). Using standard LM fitting algorithms we fitted eqn (3) to the experimental data with reasonable agreement as indicated by small and randomly distributed residuals (Fig. 1B). The systematic bias on the millisecond timescale is typically observed due to optical aberrations that cause deviations from a Gaussian observation volume, hence rendering eqn (4) only approximate. More problematic however, the LM fitting revealed a strong interdependence between the correlation rise due to antibunching and the neighbouring correlation decay as shown in Fig. 2. In a majority of experimental data sets, when the antibunching timescale and the timescale of the closest relaxation process are close, the negative amplitude antibunching term and the positive amplitude relaxation term tend to cancel each other, making it difficult to reliably fit their parameters. This is visible by poor convergence and by the fact that the solution for the two amplitudes is not unique as the one amplitude can compensate for the other. We illustrate this with experimental

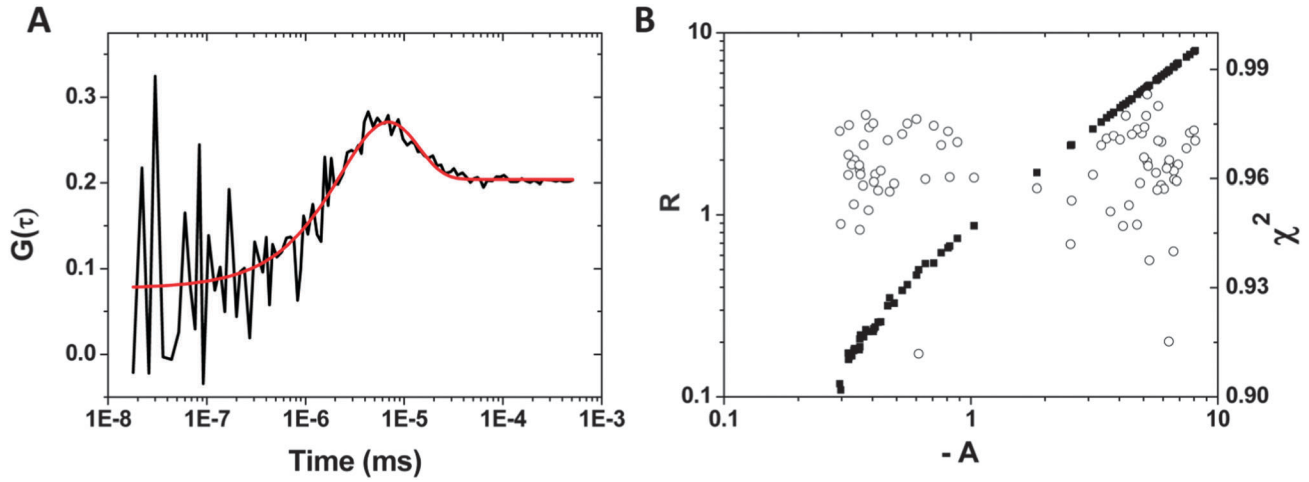

Fig. 2 FCS data measured with freely diffusing MR121 in PBS buffer with 60% sucrose at 20 °C. (A) Exemplary data curve with noise of $c = 4.4 \times 10^{-6}$ $s^{1/2}$ overlaid with a function fitted using the LM algorithm as implemented in Mathematica. The amplitudes in this particular example were estimated as $A = -4.1$ and $R = 4.0$ (which is unrealistic). (B) Fit parameter distributions showing correlations between the two amplitudes A and R (closed squares) as generated from fitting 80 experimental FCS curves using the same LM algorithm. No correlation appears between A and corresponding χ^2 values (open circles).

FCS data for pure MR121 freely diffusing in concentrated sugar solution (60% sucrose in PBS). LM fits for more than half of 80 repeated FCS measurements revealed unreasonably large and highly correlated amplitudes (Fig. 2). The effect appears to be identical whether the full data curve was analyzed or whether the data were cut off after the rotational diffusion decay excluding triplet and translational diffusion decay.

Investigating the origin of this fitting effect, we tested for a number of possible causes. First, the effect was seen in a large variety of experimental data sets collected on different setups for different samples and with different correlation algorithms. Second, the fitting artefact did not depend on starting values used in the fit routine. Third, the effect seemed to be less pronounced in simulated data. To reinforce this observation we investigated multiple sets of data simulations varying both model functions and noise contributions. In a first set of simulated FCS data, we added uncorrelated and normally distributed noise (eqn (2)) on a model function (eqn (1)). To ensure good resemblance with experimental data, we carefully characterized the noise in our experiments. Various theoretical and experimental studies revealed that noise amplitudes in multiple-tau FCS data vary with lag time and show different behavior on various time scales.[35,46,47,61–63] Since in this study we are focusing on fast time scales, we confirmed that the noise on the correlation data is Gauss-distributed with a standard deviation that scales with $\tau^{-1/2}$ for lag times in the range 18 ps to 10 μs (Fig. 1B and C). The noise amplitude c (see eqn (2)) is between 10^{-6} $s^{1/2}$ and 10^{-4} $s^{1/2}$ in typical FCS data. For instance, the data in Fig. 1 display noise with an amplitude of $c = 5.7 \times 10^{-6}$ $s^{1/2}$. Residues of all fitted curves normalized to the square root of the lag time τ and displayed as a function of τ in Fig. 1B or as a histogram with a Gaussian fit in Fig. 1C illustrate this general dependence which is independent of excitation power and integration time. The absolute noise amplitude decreases with excitation power as shown in Fig. S1 (ESI†).

We investigated noisy simulated FCS data curves generated with a model function including two parts, the antibunching phase with a characteristic rate constant of $k_{AB} = 0.4 \times 10^9$ s^{-1} and an exponential decay phase with a characteristic rate constant of $k_{rot} = 0.1 \times 10^9$ s^{-1}. Noise was added according to a noise amplitude of $c = 6 \times 10^{-6}$ $s^{1/2}$ and a representative curve is shown in Fig. S2 (ESI†). One hundred simulated data curves were fitted with a non-linear LM fitting algorithm. The distributions for the estimated fit parameters are shown in Fig. S2 (ESI†). It is revealed that the observed fitting artefact appears for data with sufficient noise and rate constants closer than a factor of ~5 albeit less pronounced than in experimental data sets.

It is important to note that in these simulations the noise on the correlation curve at various lag times is entirely uncorrelated. This, however, is not the case in real multiple-tau FCS data.[33,45,61] Therefore, in a second set of simulations, we generated correlation data by calculating the correlation of individual time trace simulations. In these simulations we assumed a Markov-state system with three distinct states that are interconnected by a transition matrix representing the rate constants for all possible transitions. By selecting certain transitions (*e.g.* only those from state 2 to state 1) as detectable, we generated single photon time traces, added Poisson-distributed background events, and calculated $G(\tau)$ using a multiple-tau algorithm as described in Materials and methods. Such data exhibit correlated noise as discussed in previous studies.[33,45] However, we found no difference in the performance of LM fitting procedures on any comparable simulation sets with uncorrelated or correlated noise.

As an alternative fitting procedure we then applied a routine to determine the dynamical fingerprints of correlation data.[35] In this routine multiple steps including independent determination of the diffusion part were carried out as described in Materials and methods. The resulting correlation curve reassembled as superposition of exponential decay functions

from all fingerprint components fitted the data equally well compared to LM fitting results as judged from the residual size and randomness (Fig. 1D). To determine the accuracy of the extracted correlation components we systematically investigated dynamical fingerprint results in experimental and simulated data.

The dynamical fingerprints determined for bimolecular interactions between MR121 and Trp as shown in Fig. 1D for solvent conditions with large viscosity exhibit positive contributions related to the antibunching signature and all decays due to rotational diffusion, PET-based quenching interactions, and intersystem crossing. Each correlation decay is reflected by a single peak in the fingerprint distribution with a width on the order of a few percent of the estimated time constant (from simulated data we estimated the width of a single peak to be around 3% of the absolute time constant for truly mono-exponential decays). This width reflects the resolution limit of the dynamical fingerprint determination under the given noise conditions in the correlation data and with the number of iterations for the fitting routine being set to 10^9. We judged the quality of a single run for determining the dynamical fingerprint of a correlation curve by five criteria: (i) size and randomness of residuals; (ii) convergence of the log-likelihood variation to a level of less than one per 1000 iterations; (iii) maximum absolute value of the likelihood; (iv) similar results in repeated runs for fingerprint determination; (v) similar results in fingerprints of repeated measurements of the correlation curve to exclude specific noise influences. Variations in the fingerprint quality depending on the number of iterations were demonstrated by analyzing experimental correlation data recorded for bimolecular interactions (Fig. S3, ESI†). We found that limiting the number of iterations to about 10^9 is a good compromise to achieve good fingerprint quality at reasonable computation time.

It should be noted that the negative amplitude of the antibunching signature is included explicitly as analytical single-exponential component in the fingerprint determination and is not displayed in the fingerprints shown in the figures. However, a spurious positive fingerprint component on the fastest time scales results in nearly all our fingerprints that is related to the antibunching component as a pure fingerprint artefact (Fig. S4, ESI†). This effect is due to the change from negative to positive decay amplitudes which cannot be entirely resolved by the fingerprint routine. It is conceivable that using a prior distribution that enforces smoothness in the fingerprint could remove this artefact.[37] In addition we found that the estimated parameters for antibunching amplitude and time constant remain close to the starting values (Fig. S4, ESI†). However, any correlation decay on larger time scales is determined independently from the antibunching fit result (and thus independent of the starting values) as long as sufficient separation in time is guaranteed and starting values for the antibunching parameters are within the range of the true values. Due to the spurious positive fingerprint peak the estimation of the amplitude and relaxation time constant for the nearest correlation decay becomes biased when the separation in time constants decreases to less than an order of magnitude.

By further studying the dynamical fingerprints of simulated correlation data, we investigated how accurate two independent exponential correlation decays are identified in the fingerprint spectrum when the gap between the two correlation decay time constants decreases. In Fig. 3 fingerprints are presented for correlation data generated from a model function like eqn (1) overlaid with noise of amplitude $c = 9 \times 10^{-6}$ $s^{1/2}$. The time constants τ_1 were varied from 10^{-8} s to 10^{-6} s while the time constant τ_2 was held constant at 10^{-7} s. It appears that separated fingerprint peaks are found as long as the correlation decay time constants are separated by at least a factor of two. The accuracy of estimated time constants is within the peak width, with a few exceptions where the relaxation times are underestimated by less than a factor of two (Fig. 3). The same behavior was found for simulated data with a larger noise constant of $c = 3 \times 10^{-5}$ $s^{1/2}$ only that the fingerprint peaks were more noisy (similar to the behavior shown in Fig. S3, ESI†). Very similar behavior was also found when the fast correlation decay approaches the antibunching time scale (Fig. S5, ESI†). Importantly, any interference between the fast correlation decay and the antibunching component does not influence estimation of the larger relaxation time if it is shifted by at least an order of magnitude.

Since the situation for experimental data on bimolecular quenching interactions is very similar, we could then analyze experimental data with good confidence. We investigated bimolecular interactions between MR121 and Trp freely diffusing in aqueous solutions with various amounts of sucrose added. An exemplary FCS data curve with fingerprint analysis was already discussed in Fig. 1. We investigated a series of measurements all performed at 20 °C in aqueous PBS solutions. Adjusting the solvent viscosity between about 1 cP and 60 cP by varying the sucrose concentration, all correlation decays were shifted towards larger times. Based on the previous validation results we determined reliable fingerprints for all bimolecular data curves (Fig. 4). At viscosities above 10 cP the rotational correlation decay appears between the antibunching signature and the PET quenching decay, increasing complexity of the FCS curve. When analyzing the data set for all viscosities with a LM fitting routine it shows that fitting can only be performed by including an exponential component for the additional rotational decay component and is always influenced by the described interdependence of fit parameters representing the amplitude for antibunching and rotational diffusional components. Since the quenching decay is spaced by more than an order of magnitude in time, both dynamical fingerprint and LM estimates for the relaxation time of the PET-quenching process should be reliable. However, we observed that LM fit estimates for the relaxation times of the quenching component are always biased towards slightly smaller values as compared to the dynamical fingerprint estimates (Fig. 5).

In addition we also found that the fingerprint routine is very sensitive to comparably small decay components that might arise from photophysical processes. Comparing data from MR121 and the structurally very similar fluorophore ATTO655 we found that ATTO655 exhibits a previously unrecognized

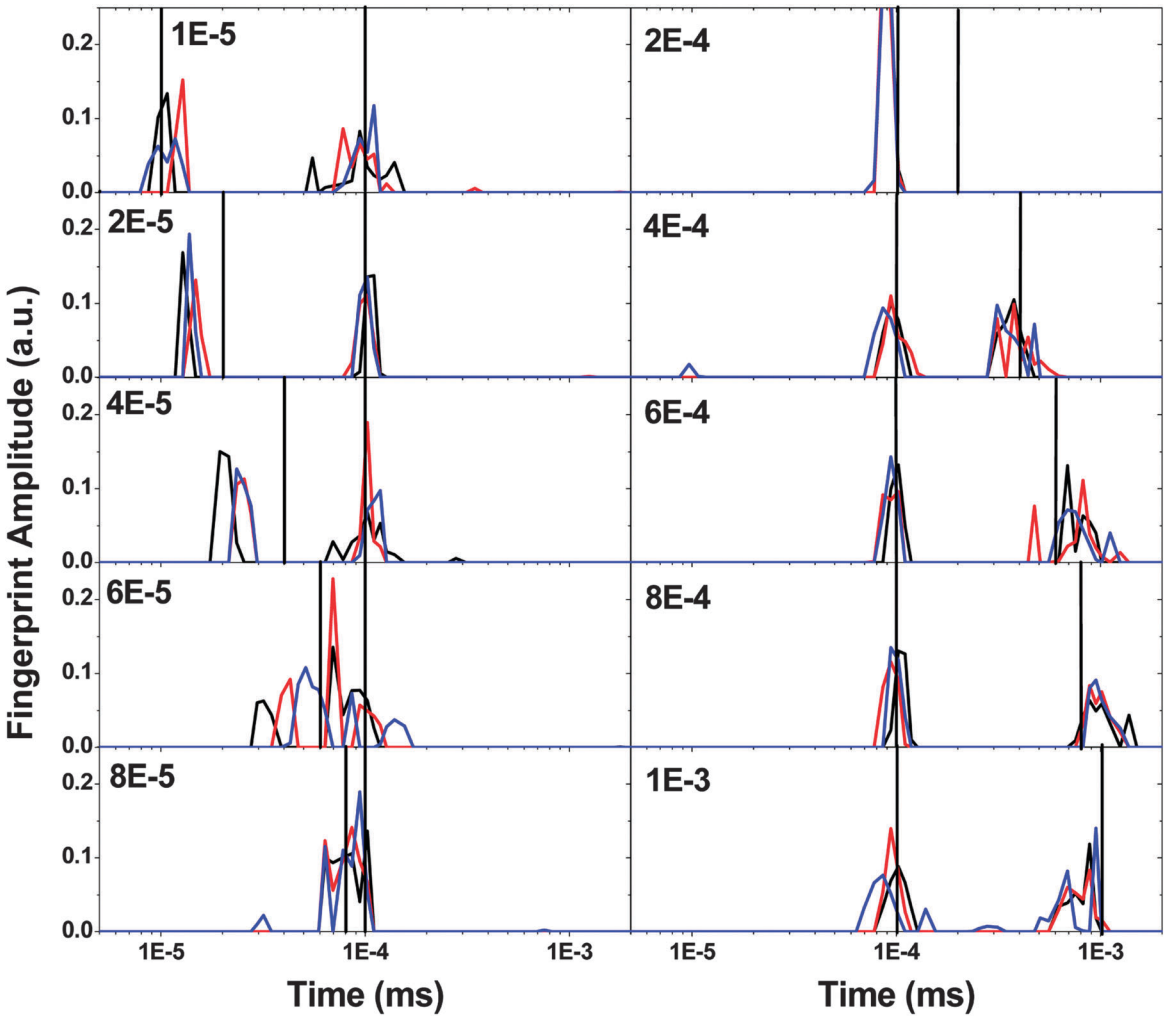

Fig. 3 Dynamical fingerprints generated for simulated FCS data. Data were simulated using the model function eqn (1) overlaid with noise following eqn (2) with a noise amplitude $c = 9 \times 10^{-6}$ $s^{1/2}$. The relaxation time of the one correlation decay was varied from 10^{-5} ms to 10^{-3} ms (as stated in the figure) while the relaxation time of the other decay was kept constant at 10^{-4} ms. The data curves in each panel show a single dynamic fingerprint for three different simulations.

correlation decay with a characteristic relaxation time between 100 ns and a few μs and with comparably small amplitude that does not appear in MR121 data. The oxazine dyes MR121 and ATTO655 were previously found to be almost identical in their photophysical characteristics including the absorption and emission spectrum, extinction coefficient, intersystem crossing rate, quantum yield, excited state life time, and PET quenching susceptibility.[40] However, when analyzing bimolecular interactions between ATTO655 and Trp at various viscosities, this previously unrecognized photophysical component clearly appears as a fingerprint peak in between those from the rotational diffusion decay and from the quenching decay. Controls showed that it is also existent in data from pure fluorophore solutions and thus is not related to interactions with Trp. Depending on the excitation power and the viscosity the photophysical peak overlays with the other peaks under certain conditions (Fig. S6, ESI†). Similar effects were also seen in peptide samples labeled with ATTO655 *via* NHS–ester coupling to the N-terminal amino group. While the origin of this additional fluorescence intermittency is unknown to us, it appears that the amplitude depends on excitation power and on solvent viscosity and the time constant is about an order of magnitude smaller than that observed for the triplet decay. The observation that variations in amplitude and time scales are similar to those of the triplet kinetics suggests a direct dependence between occupancy of triplet states and the faster unknown dark states. Further studies are underway to unravel the photophysical origin of this effect.

Discussion

This work was motivated by the quest of analyzing end-to-end contact kinetics of unstructured peptides in aqueous solution at increased viscosity. As benchmark we demonstrated the fitting performance of LM and dynamic fingerprint analysis using a sample consisting of freely diffusing fluorophore MR121/ATTO655 and quencher Trp. This model system is advantageous since no peptide properties influence the

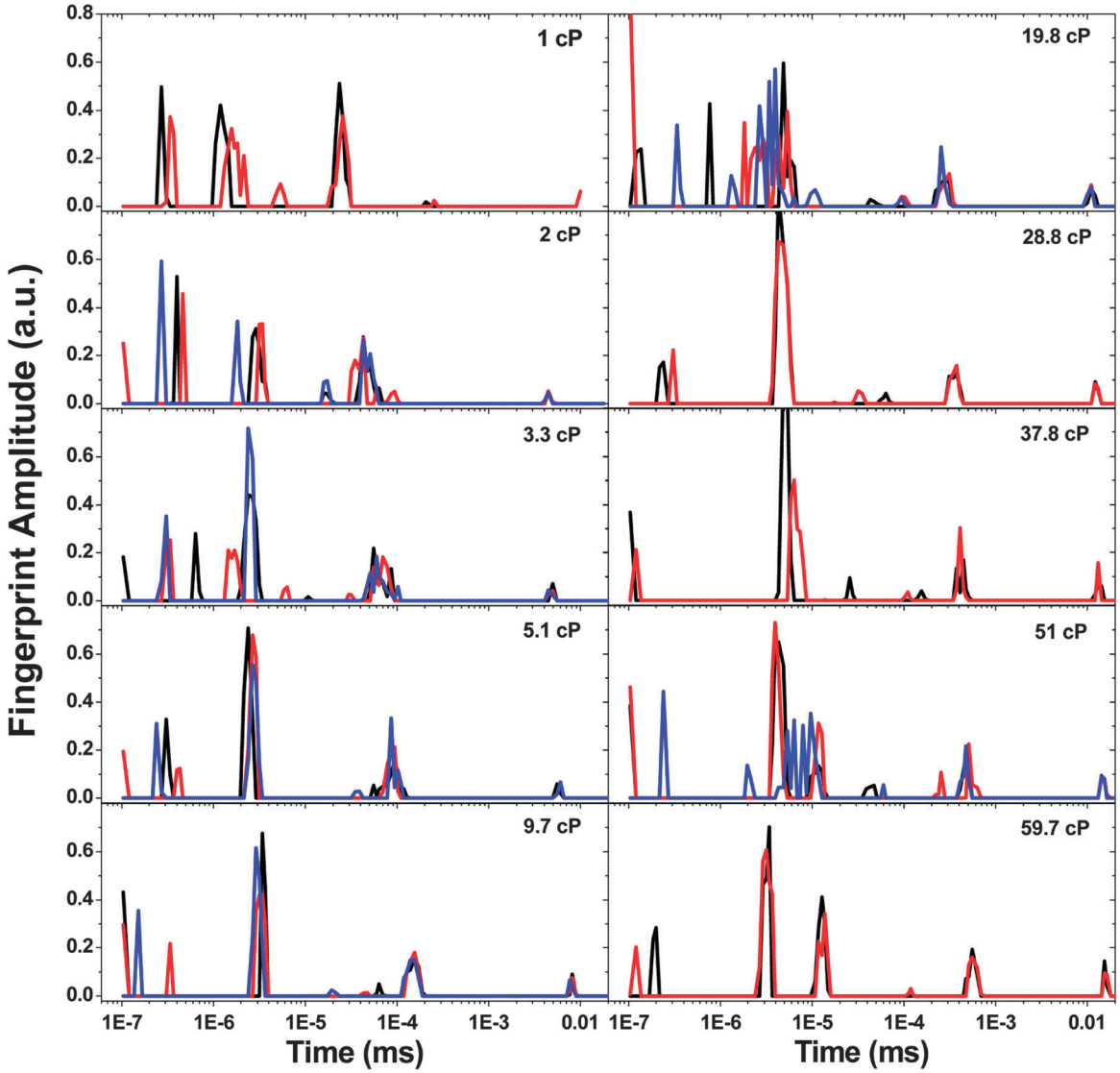

Fig. 4 Dynamical fingerprints determined for experimental FCS data that were recorded for mixtures of freely diffusing fluorophore MR121 (~1 nM) and Trp (10 mM) in PBS buffer with various concentrations of sucrose (as indicated in the figure) at 20 °C. From right to left the fingerprints reveal components due to triplet populations, quenching interactions, rotational diffusion, and antibunching artifacts. The data curves in each panel show repeated fingerprint estimates for a single FCS measurement.

observed contact-induced quenching rates; however, the various processes that introduce fluorescence fluctuation are comparable rendering the analysis procedure identical. We found that LM fitting is often compromised by the fact that the antibunching rise and the first decay partly compensate each other in most experimental data curves. The problem appears to be less pronounced with simulated data curves of multiple-tau FCS data, indicating that a minor difference between the sum of purely mono-exponential components (eqn (1)) and experimental data exists that we could not resolve. We could show that relaxation time estimates for the PET quenching interaction under experimental conditions of low viscosity, where no rotational diffusion decay is visible and the antibunching rise is well separated from the PET quenching decay, are linear as expected and identical to estimates by the dynamical fingerprint analysis. In contrast, at large viscosities, where the rotational diffusion decay is clearly visible and close to the antibunching rise, LM estimates for the relaxation time of the PET quenching interaction are biased towards smaller values as compared to dynamical fingerprint results. On the other hand, dynamical fingerprint analysis performed equally well with experimental and simulated data. The relaxation time constants for the ground-state complex formation (reported by PET quenching) as estimated by dynamical fingerprint analysis are thus reliable estimates under all conditions. They confirm the expected linear dependence between relaxation time constants and viscosity up to a viscosity of ~10 cP. At larger viscosities above 10 cP deviations towards smaller relaxation time constants for the quenching decay (Fig. 5) are also found with fingerprint analysis (thus being unrelated to detrimental

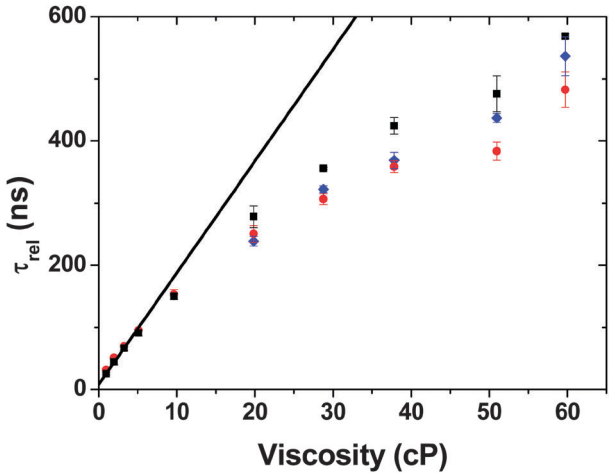

Fig. 5 Relaxation time constants as a function of solvent viscosity for bimolecular PET quenching interactions measured for freely diffusing fluorophore MR121 (~1 nM) and Trp (10 mM) in PBS/sucrose buffer at 20 °C. Time constants were estimated from dynamical fingerprint analysis (black squares), LM fitting including a term for antibunching, rotational diffusion, quenching interactions, and intersystem crossing (red circles), LM fitting of the correlation curve cut off at 6.4×10^{-9} s including a term for rotational diffusion, quenching interactions, and intersystem crossing (blue diamonds). The last procedure yielded reasonable values only for data points for viscosity < 10 cP. The straight line is a linear fit to all data points for viscosity < 10 cP.

fitting effects). The deviation is in contrast to physical expectation of a linear scaling between quenching relaxation time and viscosity for a diffusion-controlled process and must be related to the molecular reporter system.

The fact that relaxation time constants at increased viscosity above 10 cP are smaller than expected from extrapolating the linear dependence at small viscosity could be induced by a destabilization of the quenched ground-state complexes forming between fluorophore and Trp. Entanglement of association and dissociation rate constants could resolve this effect but will require precise estimates of the amplitudes for the individual decay components. We have unfortunately not yet succeeded in estimating reliable amplitude values in such complex FCS data. The ultimate goal in kinetic studies of biophysical processes is to determine the complete Markov model containing all molecular and photophysical states and the transition rate constants. Even in the simplest case of a two state system this is only possible with an accurate estimation of fingerprint amplitudes. Although the relative amplitudes in a dynamical fingerprint plot should in principle be well defined, fitting artefacts like the spurious positive peak arising from the antibunching signature prohibit a correct determination. Future work is required to improve the fingerprint algorithm to provide both relaxation rate constants and absolute amplitudes of all exponential processes.

A second possible explanation for the deviation of relaxation times from a linear viscosity dependence arises from the observation that fast PET quenching interactions with relaxation times of tens of nanoseconds appear to be slightly slower than observed by collisional quenching interactions.[40,41] It is feasible that formation of the quenched complex between the fluorophore and the quencher requires a certain time that is on the order of nanoseconds as soon as they encounter each other by translational diffusion. If the diffusional process for the encounter is slow enough, a quenched complex is formed for each encounter and the difference in time scales disappears.

In any case, this study has shown that the deviation between relaxation times estimated by the PET quenching process and a linear viscosity dependence, as previously observed with glycosylated peptides under equally large viscosities,[49] is due to the reporter system and can be even increased by a destructive fitting effect when standard LM fitting is applied.

Conclusions

We found that multiple-tau FCS data typically observed for biopolymer dynamics in viscous solution, exhibiting three or more correlation decay components on nano- to microsecond time scales, are often prone to fitting artifacts when analyzed by standard fitting routines. Both LM and dynamical fingerprint fitting is unreliable for the given noise conditions if time scales for two relaxation decays are closer than about an order of magnitude. An antibunching rise together with a correlation decay close in time are not resolved in dynamic fingerprint analysis and estimated with unrealistic and highly correlated amplitudes in LM fitting. However, we identified experimental conditions under which fitting of FCS data for bimolecular quenching interactions yields reliable data for a wide range of viscosities. Our analysis of bimolecular PET-quenching interactions reveals deviations from an expected linear scaling of quenching relaxation times with solvent viscosity towards smaller times. In addition we identified a previously unrecognized photophysical effect on the fluorescence intermittency in ATTO655 that is absent in MR121. All these results have implications for understanding end-to-end contact formation of peptides at large viscosity.

Acknowledgements

We thank K.-H. Drexhage (University of Siegen) for providing the fluorophore MR121, Oliver Reichert for technical help, and Markus Sauer for valuable discussion. We acknowledge the Deutsche Forschungsgemeinschaft (DFG) for financial support under Grant DO 1257/2-1.

Notes and references

1 E. L. Elson and D. Magde, *Biopolymers*, 1974, **13**, 1–27.
2 E. Haustein and P. Schwille, *Annu. Rev. Biophys. Biomol. Struct.*, 2007, **36**, 151–169.
3 S. T. Hess, S. Huang, A. A. Heikal and W. W. Webb, *Biochemistry*, 2002, **41**, 697–705.
4 O. Krichevsky and G. Bonnet, *Rep. Prog. Phys.*, 2002, **65**, 251–297.
5 D. Magde, E. L. Elson and W. W. Webb, *Biopolymers*, 1974, **13**, 29–61.

6 S. Maiti, U. Haupts and W. W. Webb, *Proc. Natl. Acad. Sci. U. S. A.*, 1997, **94**, 11753–11757.
7 R. Rigler and E. S. Elson, *Fluorescence correlation spectroscopy: theory and applications*, Springer-Verlag, Berlin, Heidelberg, New York, 2001.
8 K. Chattopadhyay, E. L. Elson and C. Frieden, *Proc. Natl. Acad. Sci. U. S. A.*, 2005, **102**, 2385–2389.
9 E. L. Elson, *Biophys. J.*, 2011, **101**, 2855–2870.
10 J. S. Eid, J. D. Muller and E. Gratton, *Rev. Sci. Instrum.*, 2000, **71**, 361–368.
11 S. Felekyan, R. Kuhnemuth, V. Kudryavtsev, C. Sandhagen, W. Becker and C. A. M. Seidel, *Rev. Sci. Instrum.*, 2005, **76**, 083104.
12 R. Peters, *ALV-GmbH promotional literature*, 2000.
13 K. Schätzel and R. Peters, *Proc. SPIE*, 1991, **1430**, 109–115.
14 U. Mets, in *Fluorescence Correlation Spectroscopy: theory and applications*, ed. R. Rigler and E. S. Elson, Springer-Verlag, Berlin, Heidelberg, New York, 2001, pp. 346–359.
15 U. Mets, J. Widengren and R. Rigler, *Chem. Phys.*, 1997, **218**, 191–198.
16 S. Doose, H. Neuweiler and M. Sauer, *ChemPhysChem*, 2009, **10**, 1389–1398.
17 S. Bollmann, M. Löllmann, M. Sauer and S. Doose, *Phys. Chem. Chem. Phys.*, 2011, **13**, 12874–12882.
18 H. Yang, G. Luo, P. Karnchanaphanurach, T. M. Louie, I. Rech, S. Cova, L. Xun and X. S. Xie, *Science*, 2003, **302**, 262–266.
19 X. Zhuang, T. Ha, H. D. Kim, T. Centner, S. Labeit and S. Chu, *Proc. Natl. Acad. Sci. U. S. A.*, 2000, **97**, 14241–14244.
20 C. Frieden, K. Chattopadhyay and E. L. Elson, *Adv. Protein Chem.*, 2002, **62**, 91–109.
21 O. Bieri, J. Wirz, B. Hellrung, M. Schutkowski, M. Drewello and T. Kiefhaber, *Proc. Natl. Acad. Sci. U. S. A.*, 1999, **96**, 9597–9601.
22 L. J. Lapidus, W. A. Eaton and J. Hofrichter, *Proc. Natl. Acad. Sci. U. S. A.*, 2000, **97**, 7220–7225.
23 R. R. Hudgins, F. Huang, G. Gramlich and W. M. Nau, *J. Am. Chem. Soc.*, 2002, **124**, 556–564.
24 A. C. Vaiana, H. Neuweiler, A. Schulz, J. Wolfrum, M. Sauer and J. C. Smith, *J. Am. Chem. Soc.*, 2003, **125**, 14564–14572.
25 E. Haas, *ChemPhysChem*, 2005, **6**, 858–870.
26 D. Nettels, A. Hoffmann and B. Schuler, *J. Phys. Chem. B*, 2008, **112**, 6137–6146.
27 I. V. Gopich, D. Nettels, B. Schuler and A. Szabo, *J. Chem. Phys.*, 2009, **131**, 095102.
28 J. A. Hanson and H. Yang, *J. Phys. Chem. B*, 2008, **112**, 13962–13970.
29 T. Torres and M. Levitus, *J. Phys. Chem. B*, 2007, **111**, 7392–7400.
30 B. Schuler and W. A. Eaton, *Curr. Opin. Struct. Biol.*, 2008, **18**, 16–26.
31 H. Sahoo and P. Schwille, *ChemPhysChem*, 2011, **12**, 532–541.
32 R. Rao, R. Langoju, M. Gosch, P. Rigler, A. Serov and T. Lasser, *J. Phys. Chem. A*, 2006, **110**, 10674–10682.
33 S. M. Guo, J. He, N. Monnier, G. Sun, T. Wohland and M. Bathe, *Anal. Chem.*, 2012, **84**, 3880–3888.
34 J. He, S. M. Guo and M. Bathe, *Anal. Chem.*, 2012, **84**, 3871–3879.
35 F. Noé, S. Doose, I. Daidone, M. Löllmann, M. Sauer, J. D. Chodera and J. C. Smith, *Proc. Natl. Acad. Sci. U. S. A.*, 2011, **108**, 4822–4827.
36 S. W. Provencher, *Comput. Phys. Commun.*, 1982, **27**, 229–242.
37 V. A. Voelz and V. S. Pande, *Proteins*, 2011, **80**, 335–675.
38 B. G. Keller, J.-H. Prinz and F. Noé, *Chem. Phys.*, 2012, **396**, 92–107.
39 J.-H. Prinz, B. Keller and F. Noé, *Phys. Chem. Chem. Phys.*, 2011, **13**, 16912–16927.
40 S. Doose, H. Neuweiler and M. Sauer, *ChemPhysChem*, 2005, **6**, 2277–2285.
41 H. Neuweiler, M. Löllmann, S. Doose and M. Sauer, *J. Mol. Biol.*, 2007, **365**, 856–869.
42 S. J. Hagen, *Curr. Protein Pept. Sci.*, 2010, **11**, 385–395.
43 R. Zhu, X. Li, X. S. Zhao and A. Yu, *J. Phys. Chem. B*, 2011, **115**, 5001–5007.
44 M. Mathlouthi and J. Génotelle, in *Sucrose, Properties and Applications*, ed. M. Mathlouthi and P. Reiser, Blackie Academic & Professional, 1995, pp. 126–154.
45 K. Schätzel, *Quantum Opt.*, 1990, **2**, 287–305.
46 S. Saffarian and E. L. Elson, *Biophys. J.*, 2003, **84**, 2030–2042.
47 T. Wohland, R. Rigler and H. Vogel, *Biophys. J.*, 2001, **80**, 2987–2999.
48 D. Magde, E. Elson and W. W. Webb, *Phys. Rev. Lett.*, 1972, **29**, 705–708.
49 S. Bollmann, A. Burgert, C. Plattner, L. Nagel, N. Sewald, M. Löllmann, M. Sauer and S. Doose, *ChemPhysChem*, 2011, **12**, 2907–2911.
50 S. R. Aragon and R. Pecora, *Biopolymers*, 1975, **14**, 119–137.
51 M. Ehrenberg and R. Rigler, *Q. Rev. Biophys.*, 1976, **9**, 69–81.
52 P. Kask, P. Piksarv, U. Mets, M. Pooga and E. Lippmaa, *Eur. Biophys. J.*, 1987, **14**, 257–261.
53 M. Ehrenberg and R. Rigler, *Chem. Phys.*, 1974, **4**, 390–401.
54 P. Kask, P. Piksarv, M. Pooga, U. Mets and E. Lippmaa, *Biophys. J.*, 1989, **55**, 213–220.
55 J. M. Tsay, S. Doose and S. Weiss, *J. Am. Chem. Soc.*, 2006, **128**, 1639–1647.
56 A. Loman, I. Gregor, C. Stutz, M. Mund and J. Enderlein, *Photochem. Photobiol. Sci.*, 2010, **9**, 627–636.
57 C. M. Pieper and J. Enderlein, *Chem. Phys. Lett.*, 2011, **516**, 1–11.
58 J. Widengren, in *Fluorescence Correlation Spectroscopy: theory and applications*, ed. R. Rigler and E. S. Elson, Springer-Verlag, Berlin, Heidelberg, New York, 2001, pp. 276–301.
59 K. H. Drexhage, in *Dye Lasers*, ed. F. P. Schäfer, Springer-Verlag, Berlin, Heidelberg, New York, 1973, pp. 144–179.
60 J. Widengren, U. Mets and R. Rigler, *J. Phys. Chem.*, 1995, **99**, 13368–13379.
61 D. E. Koppel, *Phys. Rev. A: At., Mol., Opt. Phys.*, 1974, **10**, 1938–1945.
62 U. Meseth, T. Wohland, R. Rigler and H. Vogel, *Biophys. J.*, 1999, **76**, 1619–1631.
63 H. Qian, *Biophys. Chem.*, 1990, **38**, 49–57.